Received: 23 November 2021 | Accepted: 12 January 2022

DOI: 10.1002/ces2.10120

International Journal of Ceramic Engineering & Science

RESEARCH ARTICLE

Microstructural and mechanical properties of geopolymers based on brick scrap and fly ash

Felix Kugler[1,3] | **Thomas Fehn**[2] | **Maximilian Sandner**[1] | **Wolfgang Krcmar**[1] | **Ulrich Teipel**[2,3]

[1] Technische-Hochschule Nürnberg, Fakultät Werkstofftechnik, Forschungsgruppe, Energieeffiziente Werkstoffe/Energie Campus Nürnberg, Nürnberg, Deutschland

[2] Technische-Hochschule Nürnberg, Fakultät Verfahrenstechnik, Fraunhofer Forschungsgruppe, Partikeltechnologie und Rohstoffinnovation, Nürnberg, Deutschland

[3] Institut für Chemieingenieurwesen, Universität Ulm, Ulm, Deutschland

Correspondence
Felix Kugler, Technische-Hochschule Nürnberg, Fakultät Werkstofftechnik, Forschungsgruppe Energieeffiziente Werkstoffe/ Energie Campus Nürnberg, Wassertorstraße 10, 90489 Nürnberg, Deutschland.
Email: felix.kugler@th-nuernberg.de

Funding information
European Commission, Grant/Award Number: LIFE18 CCM/ES/001114

Abstract

In the present work, the influence of increasing brick scrap additions on the setting behavior and material properties of fly ash-based geopolymers is investigated. The geopolymers produced are tested for their compressive strengths, bulk densities, and thermal conductivities, among other properties. Both the starting materials and the produced geopolymers are also investigated by infrared spectroscopy, X-ray diffraction analysis, and scanning electron microscopy to show the relationship between the solidification behavior and the resulting material properties. The investigations show that brick scrap is very suitable as a matrix material for geopolymer production. Increasing brick scrap additions lead, among other things, to a reduction in bulk density, thermal conductivity and compressive strength.

KEYWORDS
geopolymers, mechanical properties, microstructure, waste disposal

1 | INTRODUCTION

In 1978, J. Davidovits first mentioned geopolymers as a new class of materials.[1,2] Since then, much work has focused on the properties and potential applications of geopolymers.[3–7] Davidovits describes three different sialate monomers that are first formed in the setting reaction and then react further in a polycondensation reaction to form strength-forming structures. These are polysialate (PS: -Si-O-Al-O-), polysialatesiloxo (PSS: -Si-O-Al-O-Si-O-), and polysialatedisiloxo (PSDS: -Si-O-Al-O-Si-O-Si-O-).[1,2] Which starting monomers are formed always depends on the starting materials. Originally, geopolymers were synthesized from metakaolin and blast furnace slags. In order to produce more environmentally friendly geopolymers, fly ash was later used as an aluminosilicate carrier.[8] The use of fly ash is more environmentally friendly, as incineration and drying processes are no longer required.[9] In order to continue this environmental idea, new aluminosilicate-containing starting materials are constantly being sought which are well suited for this type of further processing. Based on this idea, studies have already

TABLE 1 X-ray fluorescence analysis of the feedstocks used fly ash (Microsit 10) and brick scrap in wt.%

Oxides	SiO_2	Al_2O_3	Fe_2O_3	CaO	MgO	K_2O	Na_2O	TiO_2
Fly ash	52.35	25.19	6.22	4.17	1.88	2.09	1.09	1.15
Brick scrap	57.43	18.57	5.91	8.61	3.08	2.81	0.77	0.86

been carried out on the production of alkali-activated materials, geopolymers, and hybrid cements from brick scrap. Thus, previous studies deal, on the one hand, with the production of alkali-activated materials from "red clay brick waste" and "granulated blast fournance slag,"[10] or on the other hand from "red clay brick" and "tungsten mining waste,"[11] from pure brick scrap[12–14] or from a combination of "red clay brick waste" with Portland cement.[13] Initial investigations into the production of geopolymers from "brick powder" and fly ash have also already been carried out.[15] In the work presented here, the brick scrap produced as a residual material in the brick industry is first ground, proportionally mixed with fly ash and, after alkaline activation, cured to form geopolymers. In particular, the influence of increasing brick dust contents on the setting behavior and material properties of the resulting geopolymer building material is investigated. The results can be used as a starting point for the targeted further development of alkali-activated binders based on residual materials with improved material properties.

2 | MATERIALS AND METHODS

2.1 | Raw materials: fly ash and brick scrap

The fly ash used, "Microsit 10," is classified as Class F fly ash with a calcium content of approx. 5%. A particle size $\times 50 = 2.9\,\mu$m of the fly ash was determined by laser diffraction. The sorted brick scrap came from a masonry brick plant and was ground in a ball mill to brick dust of particle size $\times 50 = 28.90\,\mu$m. The starting material was characterized by X-ray fluorescence analysis (XRF) and X-ray diffraction (XRD). X-ray fluorescence analysis shows the main constituents of the starting material (Table 1). The loss on ignition (LOI) determined at 950°C is 3.86 wt.% for fly ash and 0.92 wt.% for brick scrap.

XRD analysis of the fly ash shows that its crystalline portion consists mainly of mullite and quartzite, with hematite detected as a minor component. In addition to the crystalline component, the fly ash has a high amorphous component, which is evident from the X-ray amorphism in the subsurface elevation. In the XRD analysis of the brick dust, quartzite, muscovite, albite, and sodium alumina silicate are detected as major crystalline constituents and hematite as minor constituent. The brick dust present also has an amorphous phase coexisting with the crystalline phase.

TABLE 2 Composition of the investigated geopolymer mixtures

Sample	FA/BS	SiO_2/Al_2O_3	Na/Al	L/s	NaOH (g/L)
FA100	Pure FA	4.05	0.47	0.33	233
BS_1	2	4.71	0.52	0.42	233
BS_2	1	5.10	0.54	0.46	233
BS_3	0.5	5.53	0.57	0.48	233
BS_4	Pure BS	6.57	0.65	0.53	233

2.1.1 | Geopolymer synthesis

For the production of the geopolymers, the dry starting materials are mixed in different compositions and then the activator solution is added. The resulting liquid binder mixture is homogenized using a laboratory mixer. The exact compositions of the prepared geopolymer blends are listed in Table 2. By varying the solid contents of fly ash (FA) and brick dust (BS), different SiO_2/Al_2O_3 and Na/Al ratios are obtained, while the activator composition always remains the same. As the proportion of hygroscopic brick dust increases, the water requirement of the mixture increases, which is compensated by additional water to ensure consistent workability.

The respective test batches are homogenized by means of an IKA laboratory mixer of the type "RW 28 digital," operated with a spiral stirrer, over a period of time of $t = 15$ min in each case at a revolutions per minute of $u = 250$ rpm. Immediately afterward, the homogenized paste is poured into silicone molds and the air bubbles introduced are expelled on a vibrating plate over a period of $t = 5$ min. For curing, the specimens covered with PE film are stored in a drying oven at 85°C for 48 h. After the curing process, the geopolymer specimens are demolded and processed into suitable test specimens. For the compression tests, cube-shaped specimens with edge lengths ($L \times W \times H$) of 40 mm × 40 mm × 40 mm are produced. The tests for thermal conductivity $\lambda_{10,tr.}$ are performed on plate-shaped test specimens with dimensions ($L \times W \times H$) 100 mm × 100 mm × 25 mm. All test specimens that come into contact with water during processing are dried in a drying oven to constant weight and then stored in a desiccator until the material properties are measured.

2.1.2 | Activating solution

The alkaline activating solution is prepared from a liquid sodium silicate water glass of the grade "Betol 39 T" from Woellner-Werke, Ludwigshafen, in a beaker. Solid NaOH pellets are slowly added with constant stirring until the solution consists of 85.46 wt.% liquid sodium silicate and 14.54 wt.% sodium hydroxide. This activator solution is homogenized with a magnetic stirrer at a revolution per minutes of $u = 500$ rpm over a period of 24 h.

2.2 | Mechanical testing

The compressive strength or maximum compressive stress σ_d is determined in accordance with the standard DIN EN 196 Part 1. The compression test is performed with a constant pressure build-up of 1.5 N $(mm^2\ s)^{-1}$. The maximum compressive stress σ_d is calculated according to Equation (1) from the maximum applied force F and the cross-sectional area A of the test specimen. Fifteen specimens of each batch are tested to obtain a reliable average value.

$$\sigma_d = \frac{F}{A}. \tag{1}$$

For the bulk density test, the dried specimens stored in the desiccator at room temperature are weighed and the external specimen dimensions are determined. According to Equation (2), the bulk density ρ_{roh} is calculated using the mass m and the volume V of the test specimens.

$$\rho_{roh} = \frac{m}{V}. \tag{2}$$

The thermal conductivity $\lambda_{10,dr.}$ is determined according to the test standard DIN EN ISO 8302:1991 using the so-called plate method. The sample to be measured is fixed between a heating and a cooling plate and the thermal conductivities are measured at 15°C, 20°C, and 35°C sample medium temperature. Several sensors continuously determine the current temperatures of the sample surfaces. The electrical power and current required to maintain the temperatures are also determined. The thermal conductivities are calculated as a function of the respective sample medium temperatures using Equation (3), still taking into account the area A of the sample and the thickness d of the layer. Then, using linear regression, the thermal conductivity $\lambda_{10,dr.}$ at the sample medium temperature 10°C is read off. To obtain a reliable average value, three samples of each geopolymer batch are tested and the average values of thermal conductivity $\lambda_{10,dr.}$ are calculated.

$$\lambda = \frac{\dot{Q} \cdot d}{A \cdot \Delta T} = \frac{U \cdot I \cdot d}{A \cdot \Delta T}. \tag{3}$$

2.3 | Spectroscopy

2.3.1 | FT-IR spectroscopy

To visualize the structures of the produced geopolymers, Fourier transform infrared spectroscopy (FTIR) was performed on the powders using the ATR method on a Bruker Tensor II with KBr beam splitter in the spectral range 5000–400 cm^{-1}. The atmosphere was filtered out by automatic background measurements.

2.3.2 | X-ray diffraction

The mineral phase analyses of the starting materials and the produced geopolymers, determined by X-ray diffraction (XRD), are carried out with an X'Pert PRO X-ray diffractometer from Panalytical, whose cathode tube is operated with a copper anode. Generator settings of 40 mA at 45 kV are selected. The sample material is ground to a fine powder using a mortar grinder.

2.4 | Scanning electron microscopy (SEM)

In order to obtain a deeper insight into the morphology of the obtained geopolymers, images are taken using scanning electron microscopy. The fracture surfaces of the geopolymers are always examined with a 2000-fold magnification.

3 | RESULTS AND DISCUSSION

3.1 | Compressive strength

First, the compressive strengths σ_d of the different geopolymer test specimens are investigated, since a correlation between mechanical and chemical stability is suspected.[16] Figure 1 shows the compressive strengths σ_d on the primary ordinate section, which are compared on the secondary ordinate section with the corresponding SiO_2/Al_2O_3 ratios of the investigated geopolymer compositions. Here, the geopolymer type BS_1 shows the highest compressive strength with $\sigma_d = 87.6$ MPa, which is higher than the compressive strength of the geopolymer type FA_100 prepared from pure fly ash, which reaches $\sigma_d = 83.2$ MPa. Starting from the composition of the BS_1 geopolymer type, when the brick dust content and consequently the SiO_2/Al_2O_3 ratio are increased, the obtained compressive strength values decrease. For the geopolymer grade BS_2 to $\sigma_d = 73.3$ MPa and for the geopolymer grade

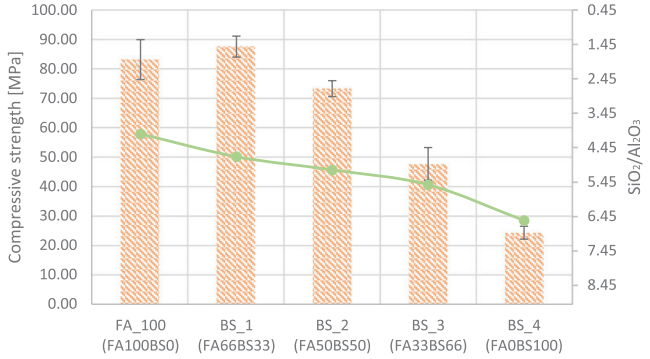

FIGURE 1 Mean values and standard deviation of compressive strengths of different types of geopolymers (FA_100, BS_1, BS_2, BS_3, BS_4) with different compositions and different SiO_2/Al_2O_3 ratios

BS_3 to $\sigma_d = 47.7$ MPa. The lowest compressive strength is exhibited by geopolymer batch BS_4 made from pure brick dust with $\sigma_d = 24.3$ MPa.

Davidovits suggested in 1999 that a SiO_2/Al_2O_3 ratio in the geopolymer between 2 and 5.5 can be used as an indicator for predicting high compressive strengths.[17] A similar SiO_2/Al_2O_3 ratio above 2.5 was also proposed by Provis and van Deventer in 2014.[18] Figure 1 shows that the FA_100 geopolymer prepared from pure fly ash has a compressive strength of 83 MPa at a SiO_2/Al_2O_3 ratio of 4. Substitution of 33 wt.% fly ash with the equivalent amount of brick powder results in an increase of the SiO_2/Al_2O_3 ratio to 4.7 and an increase of the compressive strength to 88 MPa for geopolymer BS_1. Further substitution of fly ash with brick dust leads to a steady decrease in compressive strengths with increasing SiO_2/Al_2O_3 ratio. Here, geopolymer BS_2 with a SiO_2/Al_2O_3 ratio of 5.1 exhibits a compressive strength of 73 MPa, and geopolymer BS_3 with a SiO_2/Al_2O_3 ratio of 5.5 shows a further decrease in compressive strength to 48 MPa. In the case of geopolymer batch BS_4, the fly ash was completely replaced by brick dust. As a result, the SiO_2/Al_2O_3 ratio increases to 6.6 and the compressive strength decreases to 24 MPa. Thus, the FA_100 to BS_3 compositions are within the range predicted in the literature, while the pure brick dust composition BS_4 shows a significant increase in the SiO_2/Al_2O_3 ratio beyond the range predicted as good in the literature. However, the compressive strengths of the investigated compositions first increase with an increase in the SiO_2/Al_2O_3 ratio due to the substitution of fly ash with brick dust from FA_100 to BS_1 and then decrease continuously with a further increase in the SiO_2/Al_2O_3 ratio. Based on the continuous decrease in compressive strength with increasing SiO_2/Al_2O_3 ratio, it is suggested that the increased compressive strength of composition BS_1 is due to particle strengthening of the microstructure by unreacted material, as described by Bernal[19] and Gharzouni,[20] rather than an effect of SiO_2/Al_2O_3 ratio. Accordingly, the stronger decrease in the compressive strength of the BS_4 composition of the pure brick powder composition can also be attributed to a narrower particle size distribution of the starting material due to the absence of fly ash and not to the increase of the SiO_2/Al_2O_3 ratio above the mark of 5.5 given by Davidovits.[17]

A comparison of the compressive strengths of the brick dust fly ash geopolymers measured in this work with literature data could only be carried out to a limited extent due to different chemical compositions of the starting materials and products. Similar high compressive strengths of $\sigma_d = 22$ MPa are achieved, for example, by Reig[21] for geopolymers made from "red clay brick waste (RCBW)" as in the work presented here with the geopolymer grade BS_4. By optimizing the activator solution, Reig was able to increase the compressive strength up to $\sigma_d = 50$ MPa. Also in the work of Fořt,[22] "waste brick powder" was processed with activator solutions of different compositions to geopolymers. The compressive strengths obtained ranged from $\sigma_d = 10$ MPa to $\sigma_d = 43$ MPa. Comparing the values of the pure brick powder geopolymer (BS_4) investigated here with the compressive strengths from the two aforementioned papers, they are in a similar low range with respect to their compressive strengths. The compressive strengths of all fly ash containing geopolymer compositions are significantly higher. The most comparable results were obtained by Zawrah.[23] Geopolymers were prepared and tested from "waste fired clay bricks" and "ground granulated blast-furnace-slag." Thus, compressive strengths up to $\sigma_d = 15$ MPa were obtained for geopolymers made from pure "waste fired clay bricks " and compressive strengths up to $\sigma_d = 83$ MPa were obtained in the mixture with 60 wt.% "ground granulated blast-furnace-slag" after a curing time of 90 days. In the present work, compressive strengths of 24 MPa are achieved for the geopolymers prepared from pure brick dust (BS_4), and in blend with 66 wt.% fly ash (BS_1) compressive strengths of $\sigma_d = 87$ MPa are already measured after 48 h.

3.2 | Thermal conductivity and bulk density

Figure 2 shows the results of the thermal conductivities $\lambda_{10,dr.}$ and the bulk density ρ_{roh} in graphical form. Here, the geopolymer FA_100 consisting of pure fly ash exhibits the highest bulk density of $\rho_{roh} = 1.69$ g cm^{-3} with an average thermal conductivity of $\lambda_{10,dr.} = 0.354$ W m^{-1} K^{-1}. The composition of geopolymer batch BS_1, in which 33 wt.% fly ash was replaced by brick dust, has a lower bulk density of $\rho_{roh} = 1.66$ g cm^{-3} but exhibits a higher thermal

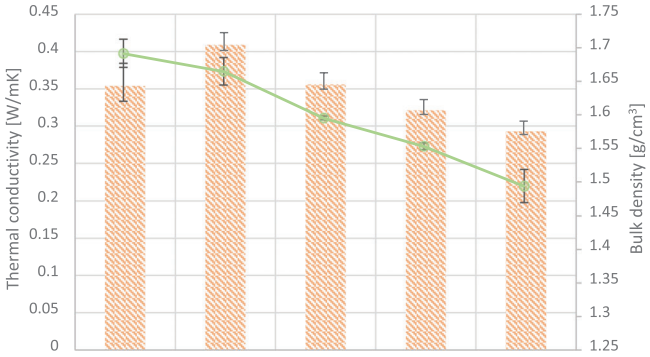

FIGURE 2 Correlation between thermal conductivities $\lambda_{10,dr.}$ and bulk densities ρ_{roh} of differently composed geopolymer batches according to formulations FA_100, BS_1, BS_2, BS_3, and BS_4

conductivity than geopolymer FA_100 with $\lambda_{10,dr.} = 0.409$ W m^{-1} K^{-1}. For the geopolymer batches where further substitution of fly ash with brick dust occurred (BS_2, BS_3, and BS_4), a continuous decrease in bulk density is observed, starting with $\rho_{roh} = 1.59$ g cm^{-3} for batch BS_2, through $\rho_{roh} = 1.55$ g cm^{-3} for batch BS_3, and finally to $\rho_{roh} = 1.49$ g cm^{-3} for batch BS_4. Corresponding to the decreasing bulk density of the geopolymer batches due to the increasing substitution of fly ash by brick dust, the associated thermal conductivities $\lambda_{10,dr.}$ also decrease proportionally. In this context, geopolymer batch BS_2 has a slightly higher thermal conductivity $\lambda_{10,dr.}$ than geopolymer batch FA_100, with a thermal conductivity of $\lambda_{10,dr.} = 0.356$ W m^{-1} K^{-1}. Geopolymer batch BS_3 has a lower thermal conductivity of $\lambda_{10,dr.} = 0.321$ W m^{-1} K^{-1}, and geopolymer batch BS_4 has the lowest thermal conductivity of the compositions investigated in this work of $\lambda_{10,dr.} = 0.293$ W m^{-1} K^{-1}.

3.3 | Structural analysis

3.3.1 | IR spectroscopy

IR spectroscopy can be used to elucidate the structures of geopolymers.[24] To detect a reaction, the IR spectra of the starting materials brick dust and fly ash (Figure 3) are compared with the IR spectra of the geopolymer batches produced from them (Figure 4). The IR spectrum of the pure fly ash shows transmission bands at wavelengths 3120, 1016, 776, and 447 cm^{-1}. The peaks at wavenumbers 1016 and 447 cm^{-1} can be assigned to the main bands of the Si-O and Al-O bonds.[25] The IR spectrum of the brick dust shows transmission bands at 1454, 1012, 777, 693, 569, and 448 cm^{-1}. Here, too, the main bands can be assigned to the same wavenumbers as for the fly ash used at 1012 and 448 cm^{-1}.[26]

The IR spectra of the investigated geopolymer batches are shown in Figure 4. The main transmission bands are at wavenumbers 3380, 980, and 440 cm^{-1}. The broad transmission band at about 3400 cm^{-1} can be attributed to the O-H groups of the silanols and the hydrogen bonds between bound water molecules and the silanols. The band at about 1650 cm^{-1} indicates water molecules bound to the inorganic geopolymer matrix. Accordingly, these transmission bands, which are not present in the starting materials, indicate newly formed silanol groups and water molecules bound into the geopolymers and can be considered an indicator that geopolymerization has occurred.[27–29]

A particularly important band related to the geopolymerization of fly ash occurs around wavenumber 1075 cm^{-1} and is also present in the IR spectrum of brick dust. This is the asymmetric vibrational bands of the Si-O-Si and Si-O-Al compounds (abbreviated Si-O-T, where T can stand for Al or Si). From literature data, it is already known that the intensity of this band is proportional to the reactivity of the starting materials.[30] In agreement with the literature, this pronounced band shifts to lower wavenumbers of about 997 cm^{-1} due to geopolymer formation. This shift clearly indicates that a chemical reaction has taken place leading to a structural change in the starting materials. The relatively strong shift of the band to lower wavenumbers can be explained by the replacement of SiO_4 tetrahedra by AlO_4 tetrahedra. This changes the chemical environment of the Si-O bonds.[2,25] If the peak shift is more pronounced, it can be assumed that more AlO_4 tetrahedra are incorporated into the SiO_4 backbone of the geopolymers, as has been observed analogously in studies of zeolites.[31–34]

In the geopolymer batches, another band appears at the wavenumber of about 1450 cm^{-1}, which is not present in the fly ash of the starting material and is hardly present in the brick dust. This band is characteristic of C-O bonds in carbonates and is probably due to the reaction of excess Na^+ ions in the activator solution with carbon dioxide from the surrounding atmosphere.[28,32] This band increases in intensity with increasing brick dust and decreasing fly ash content in the geopolymer. Therefore, it can be assumed that an increasing brick dust content favors the incorporation of unused Na^+ ions into the geopolymer matrix. The Na^+ ions are needed to saturate negatively charged AlO_4 tetrahedra, which are the main determinants of the degree of crosslinking of the geopolymer. It can be concluded that the Na^+ ions available for carbonate formation cause less crosslinking within the geopolymer matrix as the amount increases. On the one hand, this reasoning is consistent with the Na/Al ratios calculated in Section 2.1, which increase with increasing brick dust content. On the other hand, lower crosslinking of the geopolymer structure also leads to

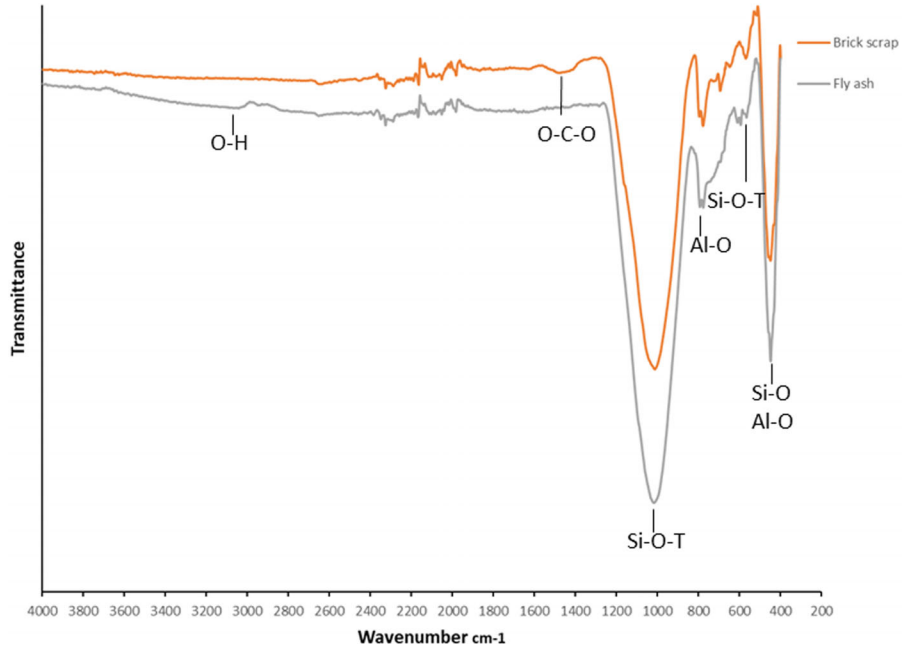

FIGURE 3 Infrared transmission spectrum of the pure feedstocks fly ash and brick dust

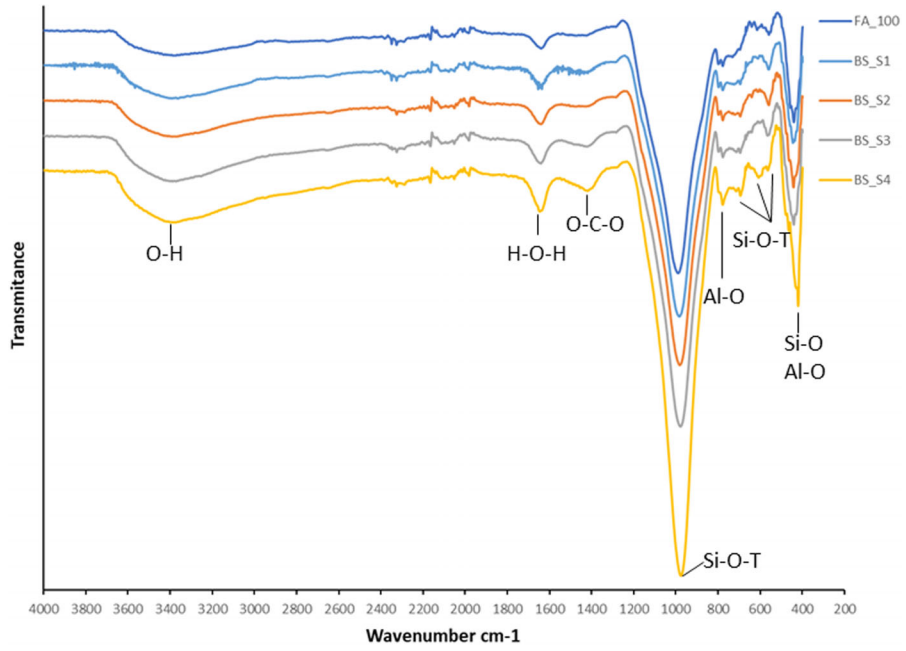

FIGURE 4 Infrared transmission spectrum of the geopolymer batches FA_100, BS_1, BS_2, BS_3, and BS_4

lower strengths, which also correlates with the results of the compressive strength measurements (Section 3.1).

3.3.2 | X-ray diffraction

The starting materials fly ash and brick dust (Figure 5A and 5B) as well as the differently composed geopolymer batches FA_100, BS_1, BS_2, BS_3, and BS_4 (Figure 6A–E) were investigated by X-ray diffraction (XRD) analysis. From these investigations, it can be deduced whether geopolymerization of the starting materials has occurred. This can be seen from the X-ray amorphous region in the XRD diagram, which is about $2\Theta = 25°$ for the fly ash used here and about $2\Theta = 26°$ for the brick dust. During polymerization, a more disordered structure is formed in the

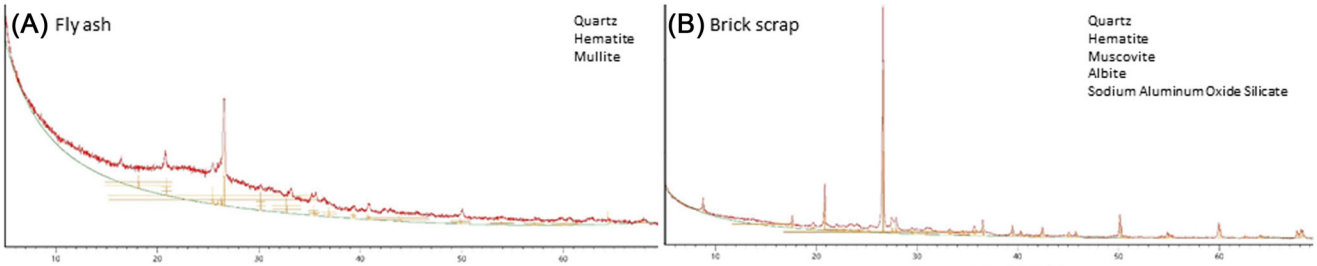

FIGURE 5 XRD diffractograms of fly ash (A) and brick dust (B)

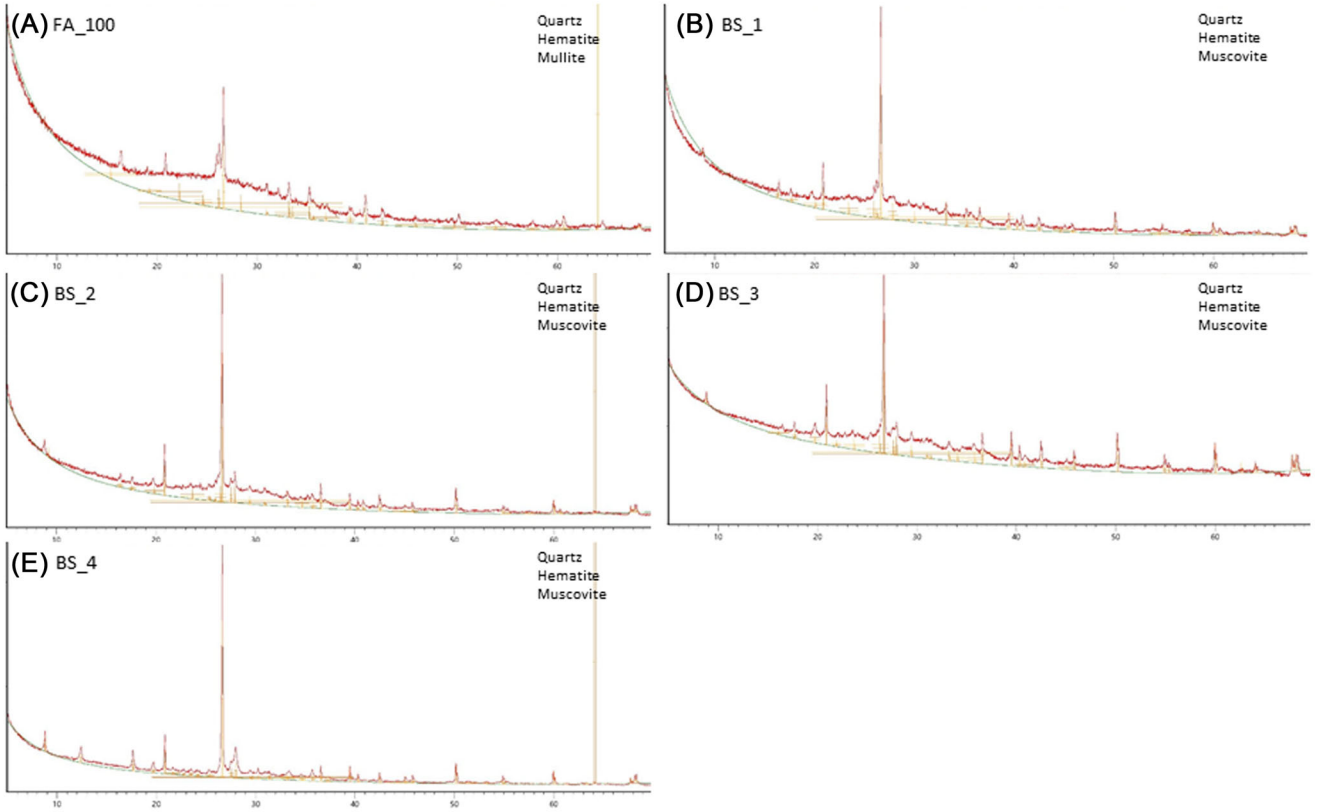

FIGURE 6 XRD diffractograms of the prepared geopolymer batches FA_100 (A), BS_1 (B), BS_2 (C), BS_3 (D), and BS_4 (E)

geopolymer matrix formed, in which the atoms are bonded further away from each other compared to the starting materials.[35] This results in a shift of the X-ray amorphous region toward higher 2Θ values.[36] Furthermore, it can be elucidated how much amorphous phase has formed in the produced geopolymer batches by qualitatively evaluating an integration of the area under the amorphous region of the respective XRD diagram.[37] In this way, a reliable statement can be made about the increase or decrease of the amorphous phase without losing the signal intensity by using a spike material, as is the case with a classical Rietveld analysis. In this way, it is also possible to elicit the mineralogical composition before and after geopolymerization from the same investigation. For this purpose, the diffraction patterns are evaluated using a database. Figure 6A–E shows the diffractograms of the investigated geopolymer batches, which are compared with the starting materials (Figure 5A and 5B). From this it can be seen that for all geopolymers the X-ray amorphous region was significantly shifted, from $2\Theta = 25°–26°$ of the starting materials to higher angles of $2\Theta = 28°–30°$. This shift in the X-ray amorphous region indicates that geopolymerization has occurred, as already expected from the results in Sections 3.1 and 3.3.1. From the integral evaluation of the areas under the X-ray amorphous regions of the reactants and the products, it is evident that the FA_100 fly ash has the highest amorphous fraction and the brick dust has the lowest amorphous fraction. The amorphous

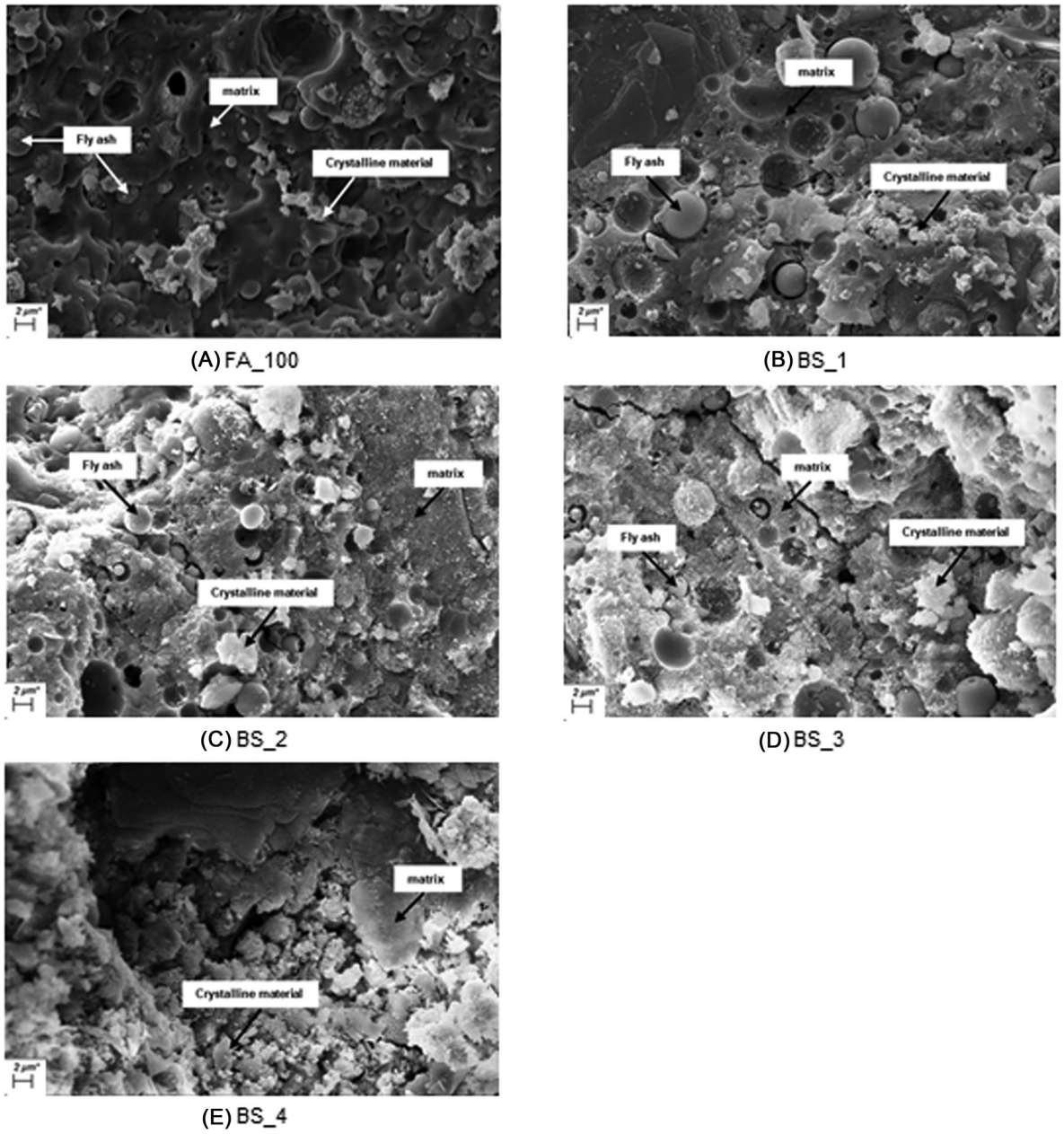

FIGURE 7 SEM images of geopolymer fracture surfaces of batches FA_100, BS_1, BS_2, BS_3, and BS_4 each in magnification 2 kx

fractions of the geopolymer batches produced are all in between. If the proportion of brick dust is increased, the mass fraction of the amorphous phase formed decreases continuously from geopolymer batch BS_1 to BS_4. It follows that with increasing brick dust content, less geopolymer matrix is formed, which explains the correlating decrease in compressive strengths. This confirms the assumption that the increased compressive strength of geopolymer batch BS_1 compared to geopolymer batch FA_100 is due to particle reinforcement, as described in Section 3.1.

3.3.3 | Scanning electron microscopy

Figure 7A–E shows the SEM images of the geopolymer fracture surfaces. Figure 7A shows the fracture surface of the pure fly ash geopolymer FA_100 with incompletely reacted round fly ash particles surrounded by matrix material. Figure 7B–E shows the geopolymer fracture surfaces with increasing brick dust content and decreasing fly ash content in the order from Figure 7B sample with 66 wt.% fly ash to Figure 7E geopolymer sample without fly ash, prepared from pure brick dust. As the fly ash content

decreases and the brick dust content increases, both the Si/Al and Na/Al ratios increase. From the comparison of the SEM images, it can be seen that with decreasing fly ash content, the number of unreacted fly ash particles also decreases. It is also evident from the comparison of the SEM images that as the brick dust content increases, the number of larger unreacted crystals introduced into the material by the brick dust itself increases. It is known from the literature that the unreacted crystals reduce the compressive strengths,[38] which is observed analogously in the present work (Section 3.1). Moreover, in the image sequence in Figure 7, the number of smaller crystals grown into the matrix increases. This can be attributed to the increasing Na/Al ratio due to the increasing brick dust content. Increasing crystal growth due to increasing Na+ ion concentration has already been reported in the literature.[5,39] From the SEM investigation, it is evident that a continuous geopolymer matrix is present in all batches containing fly ash. Even in batch BS_4 (Figure 7E), which consists of pure brick dust, the geopolymer matrix is visible. This SEM image proves to be clearly fractal and crystalline portions dominate the morphology of the fracture surface.

4 | CONCLUSION

In the work presented here, geopolymers are produced on a laboratory scale from power plant fly ash, brick dust and an alkaline activating solution with sodium water glass. The aim of the investigations was, on the one hand, to test whether brick dust is basically suitable as a matrix material for geopolymerization and what influence increasing additives have on the setting reaction and the associated material properties of the geopolymers.

All geopolymer batches of different compositions investigated here exhibit suitable compressive strengths, including the batch made from pure brick dust, designated BS_4. By means of IR spectroscopy and XRD analysis, the geopolymerization process can be clearly demonstrated. First, by the shift or new formation of transmission bands of Al-O and Si-O and O-H units when comparing the starting materials with the resulting products, which are detected by IR spectroscopy. On the other hand, XRD analysis shows that amorphous geopolymer phases form in all the compositions used here, which can be imaged by scanning electron microscope. Among other things, the study shows that the brick dust is at least partially dissolved and then participates in the geopolymer reaction. This means that pure brick dust is in principle suitable as a matrix material for geopolymers, as evidenced by the composition of the geopolymer sample BS_4 from pure brick dust. Substitution of the fly ash fraction by brick dust leads to significant changes in the material properties of the resulting geopolymers. It is found that substitution of 33 wt.% fly ash with brick dust initially increases the compressive strength to a maximum value of $\sigma_d = 87.6$ MPa due to particle reinforcement. If fly ash is further replaced by brick dust, the compressive strength decreases continuously to a minimum value of $\sigma_d = 24.3$ MPa for a geopolymer of pure brick dust. A similar behavior can be observed in the evolution of bulk densities and thermal conductivities $\lambda_{10,dr.}$. The thermal conductivity $\lambda_{10,dr.}$ of the geopolymer FA_100 from pure fly ash is $\lambda_{10,dr.} = 0.354\ W\ m^{-1}\ K^{-1}$. The substitution of 33 wt.% fly ash with brick dust initially leads to an increase in thermal conductivity to a maximum value of $\lambda_{10,dr.} = 0.409\ W\ m^{-1}\ K^{-1}$. When the brick dust content is further increased, the thermal conductivity decreases in proportion to the decreasing bulk density ρ_{roh} to a minimum of $\lambda_{10,dr.} = 0.293\ W\ m^{-1}\ K^{-1}$. The study shows that the trends in compressive strengths and thermal conductivities are in the same direction. That is, when the compressive strength is high, the thermal conductivity is also high and vice versa. This means that in the property-oriented development of geopolymers from fly ash brick powder, the tension between optimally high compressive strength or optimally low thermal conductivity should always be considered.

ACKNOWLEDGMENTS

The research leading to these results was funded by the European Union through the LIFE Program 2014–2020 for Environment and Climate Action under project number LIFE18 CCM/ES/001114.

REFERENCES

1. Davidovits J. Geopolymers: inorganic polymeric new materials. J Therm Anal. 1991;37:1633–56.
2. Davidovits J. Geopolymer: Chemistry and Applications, 5th edition. Saint-Quentin, France: Institut Géopolymère; 2020.
3. Davidovits J. Properties of geopolymer cements. In *Proceedings of the First International Conference on Alkaline Cements and Concretes*. Kiev, Ukraine: Scientific Research Institute on Binders and Materials, Kiev State University; 1994:131–49.
4. Provis JL, Palomo A, Shi C. Advances in understanding alkali-activated materials. Cem Concr Res. 2015;78:110–25.
5. van Deventer JSJ, Provis JL, Duxson P, Lukey GC. Reaction mechanisms in the geopolymeric conversion of inorganic waste to useful products. J Hazard Mater. 2007;139(3):506–13.
6. Duxson P, Fernández-Jiménez A, Provis JL, Lukey GC, Palomo A, van Deventer JSJ. Geopolymer technology: the current state of the art. J Mater Sci. 2007;42(9):2917–33.
7. Duxson P, Provis JL, Lukey GC, van Deventer JSJ. The role of inorganic polymer technology in the development of 'green concrete'. Cem Concr Res. 2007;37(12):1590–7.
8. Izquierdo M, Querol X, Davidovits J, Antenucci D, Nugteren H, Fernández-Pereira C. Coal fly ash-slag-based geopolymers:

microstructure and metal leaching. J Hazard Mater. 2009;166(1):561–6.
9. Weil M, Buchwald A, Dombrowski-Daube K. How to assess the environmental sustainability of geopolymers? A live cycle perspective. AST. 2010;69:186–91.
10. Rakhimova NR, Rakhimov RZ. Alkali-activated cements and mortars based on blast furnace slag and red clay brick waste. Mater Design. 2015;85:324–31.
11. Sedira N, Castro-Gomes J, Magrinho M. Red clay brick and tungsten mining waste-based alkali-activated binder: microstructural and mechanical properties. Constr Build Mater. 2018;190:1034–48.
12. Komnitsas K, Zaharaki D, Vlachou A, Bartzas G, Galetakis M. Effect of synthesis parameters on the quality of construction and demolition wastes (CDW) geopolymers. Adv Powder Technol. 2015;26(2):368–76.
13. Robayo RA, Mulford A, Munera J, Mejía de Gutiérrez R. Alternative cements based on alkali-activated red clay brick waste. Constr Build Mater. 2016;128:163–9.
14. Robayo-Salazar RA, Mejía-Arcila JM, Mejía de Gutiérrez R. Eco-efficient alkali-activated cement based on red clay brick wastes suitable for the manufacturing of building materials. J Cleaner Prod. 2017;166:242–52.
15. Rovnaník P, Řezník B, Rovnaníková P. Blended alkali-activated fly ash /brick powder materials. Procedia Eng. 2016;151:108–13.
16. Kränzlein E, Harmel J, Pöllmann H, Krcmar W. Influence of the Si/Al ratio in geopolymers on the stability against acidic attack and the immobilization of Pb2+ and Zn2+. Constr Build Mater. 2019;227:116634.
17. Davidovits J, editor. Proceedings of the '99 Geopolymer International Conference: June 30 to July 2, 1999, Saint-Quentin, France. [Elektronische Ressource]. Saint Quentin: Geopolymer Institute; 2003.
18. Provis JL, van Deventer JSJ, editors. Alkali Activated Materials: State-of-the-Art Report, RILEM TC 224-AAM. Dordrecht: Springer; 2014. (RILEM State-of-the-Art Reportsvolume 13).
19. Bernal SA, Bejarano J, Garzón C, Mejía de Gutiérrez R, Delvasto S, Rodríguez ED. Performance of refractory aluminosilicate particle/fiber-reinforced geopolymer composites. Compos Part B: Eng. 2012;43(4):1919–28.
20. Gharzouni A, Sobrados I, Joussein E, Baklouti S, Rossignol S. Predictive tools to control the structure and the properties of metakaolin based geopolymer materials. Colloids Surf A. 2016;511:212–21.
21. Reig L, Tashima MM, Borrachero MV, Monzó J, Cheeseman CR, Payá J. Properties and microstructure of alkali-activated red clay brick waste. Constr Build Mater. 2013;43:98–106.
22. Fořt J, Vejmelková E, Koňáková D, Alblová N, Čáchová M, Keppert M, et al. Application of waste brick powder in alkali activated aluminosilicates: functional and environmental aspects. J Cleaner Prod. 2018;194:714–25.
23. Zawrah MF, Gado RA, Feltin N, Ducourtieux S, Devoille L. Recycling and utilization assessment of waste fired clay bricks (Grog) with granulated blast-furnace slag for geopolymer production. Process Saf Environ Prot. 2016;103:237–51.
24. Lee WKW, van Deventer JSJ. Use of infrared spectroscopy to study geopolymerization of heterogeneous amorphous aluminosilicates. Langmuir. 2003;19(21):8726–34.
25. Bohra VKJ, Nerella R, Madduru SRC, Rohith P. Microstructural characterization of fly ash based geopolymer. Mater Today: Proc. 2020;27:1625–9.
26. Djomgoue P, Njopwouo D. FT-IR spectroscopy applied for surface clays characterization. JSEMAT. 2013;03(04):275–82.
27. Nath DCD, Bandyopadhyay S, Gupta S, Yu A, Blackburn D, White C. Surface-coated fly ash used as filler in biodegradable poly(vinyl alcohol) composite films: part 1—the modification process. Appl Surf Sci. 2010;256(9):2759–63.
28. Nayak PS, Singh BK. Instrumental characterization of clay by XRF, XRD and FTIR. Bull Mater Sci. 2007;30(3):235–8.
29. Zhang Z, Wang H, Provis JL. Quantitative study of the reactivity of fly ash in geopolymerization by FTIR. J Sustain Cement-Based Mater. 2012;1(4):154–66.
30. Khale D, Chaudhary R. Mechanism of geopolymerization and factors influencing its development: a review. J Mater Sci. 2007;42(3):729–46.
31. Alvarez-Ayuso E, Querol X, Plana F, Alastuey A, Moreno N, Izquierdo M et al. Environmental, physical and structural characterisation of geopolymer matrixes synthesised from coal (co-)combustion fly ashes. J Hazard Mater. 2008;154(1–3):175–83.
32. Klinowski J. Nuclear magnetic resonance studies of zeolites. Prog Nucl Magn Reson Spectrosc. 1984;16:237–309.
33. Kramar S, Ducman V. Mechanical and microstructural characterization of geopolymer synthesized from low calcium fly ash. CI&CEQ. 2015;21(1–1):13–22.
34. Motorwala A, Shah V, Kammula R, Nannapaneni P, Raijiwala, DB. Alkali activated fly-ash based geopolymer concrete. Int J Emerg Technol Adv Eng. 2013;3(1):159–66.
35. Provis JL. Geopolymers and other alkali activated materials: why, how, and what? Mater Struct. 2014;47(1–2):11–25.
36. Rattanasak U, Chindaprasirt P. Influence of NaOH solution on the synthesis of fly ash geopolymer. Miner Eng. 2009;22(12):1073–8.
37. Schneider C, Baetzner S. X-ray diffractometric determination of the granulated blastfurnace slag content of cement. Cement Int. 2005;3:96–105.
38. Ahmad S, Iqbal Y, Ghani F. Phase and microstructure of brick-clay soil and fired clay-bricks from some areas in Peshawar Pakistan. J Pakistan Mater Soc. 2008;1:33–9.
39. Provis JL, Bernal SA. Geopolymers and related alkali-activated materials. Annu Rev Mater Res. 2014;44(1):299–327.

How to cite this article: Kugler F, Fehn T, Sandner M, Krcmar W, Teipel U. Microstructural and mechanical properties of geopolymers based on brick scrap and fly ash. Int J Ceramic Eng Sci. 2022;1–10. https://doi.org/10.1002/ces2.10120